



LAWRENCE  
LIVERMORE  
NATIONAL  
LABORATORY

# Images of the gold bubble feature from ViewFactor experiments at the National Ignition Facility

M. B. Schneider, S. A. Maclaren, K. Widmann, J. Hammer

November 21, 2013

8th International Conference on Inertial Fusion Sciences and Applications (IFSA 2013)  
Nara, Japan  
September 8, 2013 through September 13, 2013

## **Disclaimer**

---

This document was prepared as an account of work sponsored by an agency of the United States government. Neither the United States government nor Lawrence Livermore National Security, LLC, nor any of their employees makes any warranty, expressed or implied, or assumes any legal liability or responsibility for the accuracy, completeness, or usefulness of any information, apparatus, product, or process disclosed, or represents that its use would not infringe privately owned rights. Reference herein to any specific commercial product, process, or service by trade name, trademark, manufacturer, or otherwise does not necessarily constitute or imply its endorsement, recommendation, or favoring by the United States government or Lawrence Livermore National Security, LLC. The views and opinions of authors expressed herein do not necessarily state or reflect those of the United States government or Lawrence Livermore National Security, LLC, and shall not be used for advertising or product endorsement purposes.

# Images of the gold bubble feature from ViewFactor experiments at the National Ignition Facility

M. B. Schneider<sup>1</sup>, S. A. MacLaren<sup>1</sup>, K. Widmann<sup>1</sup>, N. B. Meezan<sup>1</sup>, J. H. Hammer<sup>1</sup>, B. E. Yoxall<sup>1</sup>, P. M. Bell<sup>1</sup>, D. K. Bradley<sup>1</sup>, D. A. Callahan<sup>1</sup>, M. J. Edwards<sup>1</sup>, T. M. Guymer<sup>2</sup>, D. E. Hinkel<sup>1</sup>, W. W. Hsing<sup>1</sup>, M. L. Kervin<sup>1</sup>, J. D. Moody<sup>1</sup>, A. S. Moore<sup>2</sup>, O. L. Landen<sup>1</sup>, N. E. Palmer<sup>1</sup>, A. T. Teruya<sup>1</sup>

<sup>1</sup>Lawrence Livermore National Laboratory, P.O. Box 808, Livermore, CA 94550, USA

<sup>2</sup>Atomic Weapons Establishment, Aldermaston, Reading RG7 4PR, UK

E-mail: [schneider5@llnl.gov](mailto:schneider5@llnl.gov)

## Abstract.

The ViewFactor experiments at the National Ignition Facility use a truncated hohlraum to allow excellent diagnostic views of the interior of the hohlraum. Time-integrated, hard x-ray (3 - 5 keV) images show the region where the laser deposits its energy at peak power. These images show a three-dimensional structure in the region where the outer beams deposit their energy (the “gold bubble”) which varies with pulse shape and cross beam energy transfer. The images from two-dimensional simulations have similar trends but show some discrepancies.

## 1. Introduction

The National Ignition Facility (NIF)[1] at Lawrence Livermore National Laboratory is currently engaged in the pursuit of fusion ignition using indirect drive inertial confinement fusion (ICF)[2]. Up to 1.8 MJ and 500 TW of laser energy and power from the NIF, a 192 beam, 351 nm Nd glass laser, is converted to a tailored x-ray drive in a cryogenic gas-filled gold hohlraum. The drive implodes the capsule in its center which has a doped plastic (CH) ablator surrounding the deuterium-tritium fuel.[3] Measured ablator implosion velocity is observed to be slow relative to simulations[4],[5] but these measurements could not determine if this was due to an x-ray drive deficit or capsule physics.

The ViewFactor experiment was designed[6] to determine if the slower implosion velocity was due to an x-ray drive deficit. These experiments use an ignition hohlraum with one end truncated (see Figure 1a) to allow views of the hohlraum interior from the capsule point-of-view.[7] The drive irradiance measured through the open end, which needs no source size correction, was 70-85% of that predicted by the model[7] and thus explains nearly all of the velocity deficit.

The open end allows diagnostics a complete view of the hohlraum interior, and we focus this paper on the time-integrated images of the hohlraum interior at 18° to the hohlraum axis, (see Figure 1b) in an x-ray energy band of 3-5 keV. These are images of the regions in which the laser deposits its energy at peak power.

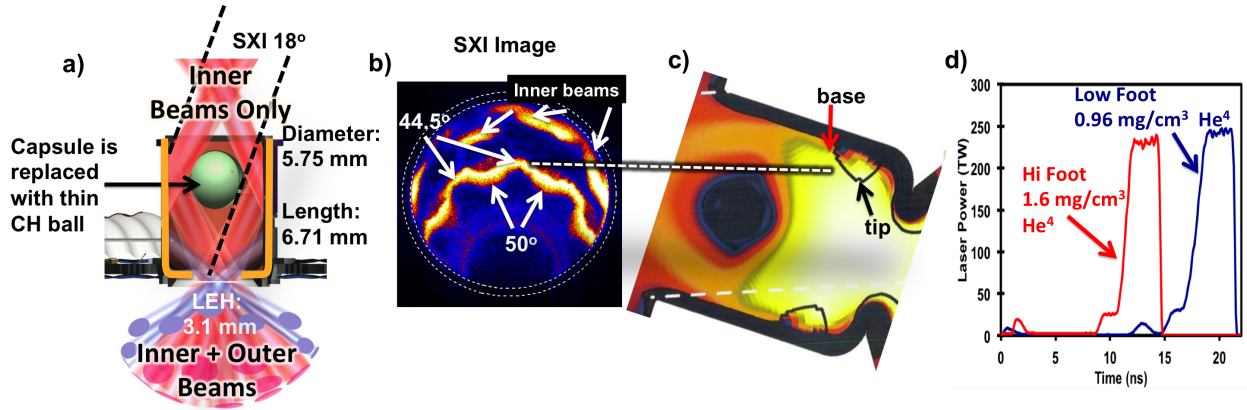


**Figure 1.** The experimental configuration. (a) The ViewFactor target showing the truncated “open” end facing up and the LEH end facing down. (b) Typical time-integrated SXI image taken in an x-ray energy band of 3-5 keV and viewing the hohlraum at  $18^\circ$  to its axis. (c) Map of electron temperature at time of maximum power from a HYDRA[8] simulation. The map is tilted  $18^\circ$  to identify features in the SXI image. Horizontal line shows the gold bubble feature. The tip and base of the bubble are defined. (d) Plot of laser power vs. time.

## 2. Experimental Description

The nominal ignition hohlraum is 5.75 mm in diameter, 9.425 mm long, with 3.1 mm diameter laser entrance holes (LEHs). The ViewFactor target has one half identical to the ignition hohlraum, but the other half extends only 2 mm beyond the hohlraum center, with an opening equal to the full diameter of the hohlraum as shown in Figure 1a. The ViewFactor target is shot at cryogenic temperature and is filled with He gas at the same mass density as in the corresponding ignition design. The fuel capsule is replaced by a thin plastic spherical shell (3 mm diameter with 20 or 30  $\mu\text{m}$  shell thickness). There are several holes in the CH shell so that its interior has same mass density as the hohlraum. The thin shell is nearly completely ablated by the peak of the drive. ViewFactor experiments were done in pairs, open-end down and open-end up, so all diagnostics obtained data looking into both the open end and the LEH end.

The hohlraum is driven with one of two standard ignition pulse shapes, a low foot pulse or a high foot pulse, which are shown in Figure 1d. The full complement of 96 beams (64 outer beams at  $44.5^\circ$  and  $50^\circ$  to the hohlraum axis) and 32 inner beams ( $23.5^\circ$  and  $30^\circ$  to the hohlraum axis) is used at the LEH side but only the 32 inner beams are used at the open end. The relative power between the inner and outer beams at the LEH end can be adjusted by transferring energy from the outer to the inner beams by tuning the laser wavelength difference between them.[9] This is called cross beam energy transfer (CBET).

Four experiments are discussed here. The first experiment used a 20  $\mu\text{m}$  thick CH shell, a low-foot laser pulse, and a wavelength separation of 7.9A (9.1A) between the  $30^\circ$  ( $23.5^\circ$ ) and outer beams. The second experiment was identical to this except the CH shell was 30  $\mu\text{m}$  thick. The third experiment was identical to the second experiment except the wavelength separations were reduced to 1.5 A to lower the amount of CBET to near zero. The fourth experiment used a hi-foot laser pulse with 7.3A (8.5A) wavelength separation.

This paper focuses on the images obtained with the the Static X-ray Imager (SXI), a pinhole camera with an x-ray CCD detector.[10] It views the hohlraum at  $18^\circ$  to the its axis from the upper hemisphere. It has a hard channel sensitive to 3 to 5 keV x-rays defined by a titanium filter. The filters in SXI are not calibrated, so the images are normalized to the signal levels

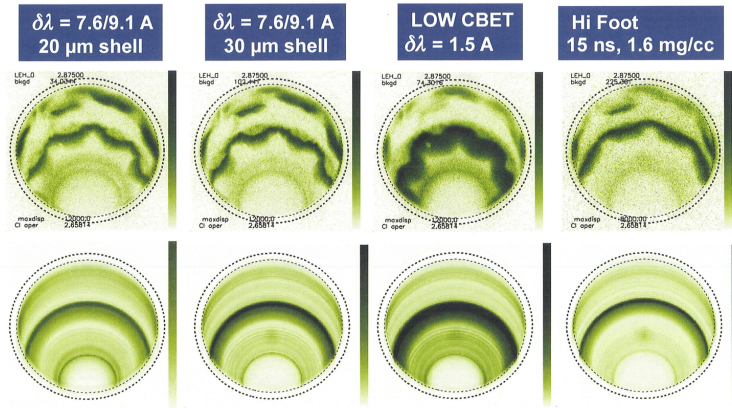


**Figure 2.** SXI images of data (top row) and model (bottom row).

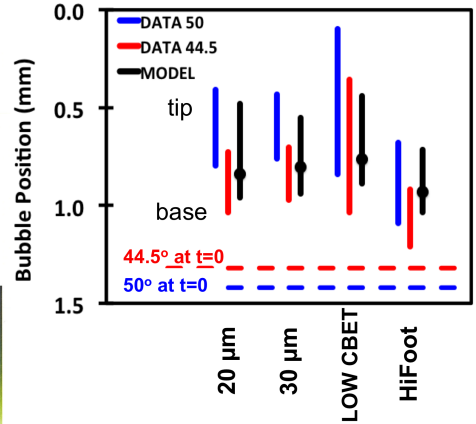


**Figure 3.** Plot of location of bubble (base to tip) in SXI image. The brightest part of bubble in model is marked.

in the 4 keV x-ray channel of the Dante diagnostic[11], a time-resolved, low resolution x-ray spectrometer which views the hohlraum from the lower hemisphere at  $37^\circ$  to its axis. Figure 1b and c show a typical SXI image and a simulated map of electron temperature. The map is used to identify the gold bubble feature formed by the outer beams. Figure 2, top row, shows the normalized images from the four experiments.

### 3. Modelling

The ViewFactor experiments were modeled[7] with the LASNEX code[12] using the High Flux Model[13]. This model uses a flux limiter on the Spitzer formula for electron conduction of  $f = 0.15$  and it uses the detailed configuration accounting (DCA) non-local thermodynamic equilibrium (NLTE) atomic physics model[14] to generate the opacities responsible for emission. The simulation is first run using the measured laser energy to establish plasma conditions. The CBET is calculated for these plasma conditions, the laser pulses are modified using this CBET and the measured backscatter, and the model is run again[15].

To compare to the data, a post shot simulation was run using the measured laser drive minus the backscatter. These simulations have been post-processed to produce DANTE voltages and SXI images. The normalized simulated SXI images are shown in Figure 2, bottom row.

### 4. Results

The data in Figure 2 top row shows that the gold bubble pattern is three-dimensional, with the bubble from the  $50^\circ$  beams growing more than that from the  $44.5^\circ$  beams. This cannot be captured in the images from the two-dimensional models, shown in the bottom row. However, the modeled images do look similar to the data. For instance, comparing the second and third experiments whose only different is CBET vs LOW CBET, respectively, the bubble regions are wider in LOW CBET images because energy is not lost from the outer beams.

More insight can be gained by measuring the position of the bubble tips and bases, as defined in Figure 1c. The position is defined as the location of the point of half the maximum intensity. Each series of tips or bases in the SXI image is fit to a circle foreshortened by  $18^\circ$ . The position of the tip (or base) is defined as the vertical distance from the top of the circle to the middle of the SXI image. The positions of the bubbles (base to tip) are plotted in Figure 3 for all the images shown in Figure 2. The model predicts the position of the bubble correctly, especially for

the first two experiments (low foot pulse with CBET). However, the model predicts the LOW CBET bubble width to be only 65% of the measured width.

The inner beams in the data images in Figure 2 look brighter than those in the model, except for the LOW CBET shot. To quantify this, the total counts in the inner and outer beam regions are measured. Figure 4 shows the definition of the region of inner beams (outlined in red) and outer beams (outlined in blue). The ratio of the total counts in the inner beam region to that in the outer beam region is calculated and plotted. Both data and model see a decrease in inner to outer beam ratio in going to the thicker capsule. This, plus the increase in laser backscatter[7], is an indication of the influence of capsule blow-off on plasma conditions. Figure 4 shows that the model underestimates the ratio for the two low foot experiments with CBET and the HiFoot experiment but agrees with the data for the LOW CBET experiment. This may indicate an issue in the way CBET is implemented in the model.

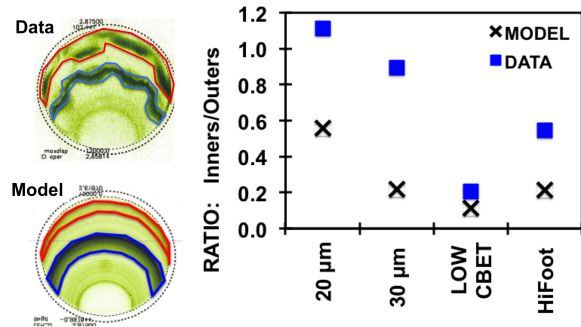


**Figure 4.** Ratio inner/outer beam brightness.

## 5. Conclusion

The ViewFactor experiment allows excellent diagnostic views of the interior of an ignition hohlraum. Time-integrated images in the 3-5 keV x-ray range at  $18^\circ$  to the hohlraum axis show the region in which the outer beams deposit their energy at peak power, the gold “bubble” is three-dimensional. The two-dimensional models produce images that are similar to the data but they underestimate the size of the bubble when there is LOW CBET and they underestimate the brightness of the inner beams when there is CBET. Three-dimensional models are in progress[16] as are enhancements to the current models, such as an in-line CBET package[17].

## 6. Acknowledgments

The authors gratefully acknowledge the efforts of the NIF Operations, Laser Performance, Target Diagnostics, and Target Fabrication Teams. This work was performed under the auspices of the Lawrence Livermore National Security, LLC, (LLNS) under Contract No. DE-AC52-07NA27344.

- [1] Moses E *et al.* 2009 *Phys. Plasmas* **16** 041006
- [2] Lindl J *et al.* 2004 *Phys. Plasmas* **11** 339
- [3] Haan S W *et al.* 2011 *Phys Plasmas* **18** 051001
- [4] Hicks D G *et al.* 2012 *Phys Plasmas* **19** 122702
- [5] Meezan N *et al.* 2013 *Phys. Plasmas* **20** 056311
- [6] Hammer J 2013 *These proceedings*
- [7] Maclaren S A *et al.* 2013 *Phys Rev Lett.* **submitted** sub
- [8] Marinak M M 2001 *Phys Plasmas* **8** 2275
- [9] Michel P *et al.* 2009 *Phys. Plasmas* **16** 042702
- [10] Schneider M B *et al.* 2010 *Rev. Sci. Instrum* **81** 10E358
- [11] Kline J *et al.* 2010 *Rev. Sci. Instrum.* **81** 10E538
- [12] Zimmerman G B and Kruer W L 1975 *Comments Plasma Phys. Controlled Fusion* **2** 51
- [13] Rosen M D *et al.* 2011 *High Energy Density Physics* **7** 180
- [14] Scott H and Hansen S 2010 *High Energy Density Phys.* **6** 39
- [15] Town R P J *et al.* 2011 *Phys. Plasmas* **18** 056302
- [16] Meezan N 2013 personal communication
- [17] Marinak M and Meezan N 2013 personal communication